Available online at www.sciencedirect.com
SCIENCE DIRECT®
Microporous and Mesoporous Materials 78 (2005) 225–234
MICROPOROUS AND MESOPOROUS MATERIALS
www.elsevier.com/locate/micromeso

Chiral open-framework uranyl molybdates. 3. Synthesis, structure and the $C222_1 \rightarrow P2_12_12_1$ low-temperature phase transition of $[C_6H_{16}N]_2[(UO_2)_6(MoO_4)_7(H_2O)_2](H_2O)_2$

Sergey V. Krivovichev [a,*], Th. Armbruster [b,c], Dmitry Yu. Chernyshov [b,c], Peter C. Burns [d], Evgeniy V. Nazarchuk [a], Wulf Depmeier [e]

[a] Department of Crystallography, St. Petersburg State University, University Emb. 7/9, 199034 St. Petersburg, Russia
[b] Laboratorium für chemische and mineralogische Kristallographie, Universität Bern, Freiestrasse 3, CH-3102 Bern, Switzerland
[c] Petersburg Nuclear Physics Institute, Orlova Grove, Gatchina, Leningrad District 188350, Russia
[d] Department of Civil Engineering and Geological Sciences, University of Notre Dame, 156 Fitzpatrick Hall, Notre Dame, IN 46556, USA
[e] Institut für Geowissenschaften, Kiel Universität, Olshausenstrasse 40, D-24118 Kiel, Germany

Received 5 April 2004; received in revised form 7 October 2004; accepted 8 October 2004
Available online 30 November 2004

Abstract

A new chiral 6:7 open-framework uranyl molybdate, $[C_6H_{16}N]_2[(UO_2)_6(MoO_4)_7(H_2O)_2](H_2O)_2$, has been synthesized by hydrothermal methods. The structure has been refined using single-crystal X-ray diffraction data collected at 20 and −127 °C. The 20 °C structure [orthorhombic, $C222_1$, $a = 11.3045(14)$, $b = 19.962(6)$, $c = 24.416(5)$ Å, $V = 5510(2)$ Å^3] has been refined to $R_1 = 0.046$ on the basis of 6093 unique observed reflections. The −127 °C structure [orthorhombic, $P2_12_12_1$, $a = 11.211(4)$, $b = 19.880(10)$, $c = 24.421(8)$ Å, $V = 5443(4)$ Å^3] has been refined to $R_1 = 0.047$ on the basis of 6951 unique observed reflections. The structures are based upon topologically identical frameworks of corner-sharing UO_7 pentagonal bipyramids and MoO_4 tetrahedra. The extra-framework H_2O groups and protonated triethylamine molecules reside in the framework cavities. In the $C222_1$ structure at 20 °C, H_2O and $[C_6H_{16}N]^+$ molecules filling the chiral channels along [0 0 1] are disordered, whereas, in the $P2_12_12_1$ structure at −127 °C, they are perfectly ordered. The symmetry difference between structures at 20 °C and −127 °C is the result of a $C222_1 \rightarrow P2_12_12_1$ second order phase transition that involves ordering of extra-framework protonated amine molecules and H_2O groups, and distortion of the flexible $[(UO_2)_6(MoO_4)_7(H_2O)_2]^{2-}$ uranyl molybdate framework. On the basis of measurements of intensities of reflections that violate absence conditions of C-centering cell, the temperature of the phase transition is estimated as −11 °C.

Keywords: Uranyl molybdates; Open framework; Crystal structure; Phase transition; Order–disorder

1. Introduction

Chiral open-framework uranyl molybdates are of potential interest for a number of applications, including ion-exchange, catalysis and radioactive waste remediation [1–3]. They also represent an interesting group of materials that are based upon heteropolyhedral frameworks with corner-sharing between polyhedra of different types. In the case of uranyl molybdates, UO_7 pentagonal bipyramids and MoO_4 tetrahedra are the most common structural subunits. The U–O_{br}–Mo links (O_{br} = bridging oxygen atoms) are flexible and result in observed interesting physical behavior of structures of

* Corresponding author. Address: Institute für Mineralogie and Petrographie, Leopold-Franzens-Universität Innsbruck, Innrain 52, Innsbruck 6020, Austria.
E-mail address: skrivovi@mail.ru (S.V. Krivovichev).

1387-1811/$ - see front matter © 2004 Elsevier Inc. All rights reserved.
doi:10.1016/j.micromeso.2004.10.020

uranyl molybdates such as highly anisotropic thermal expansion and phase transitions [4]. As shown in [3], uranyl molybdate frameworks are sufficiently flexible to be able to adapt to the geometrical shape of extra-framework cations.

In this paper, we report the synthesis, structure and low-temperature phase transition of $[C_6H_{16}N]_2[(UO_2)_6(MoO_4)_7(H_2O)_2](H_2O)_2$, a new chiral open-framework uranyl molybdate with protonated amine molecules within framework cavities. The flexibility of the framework allows the structure to adapt to different degrees of order of the guest molecules during the structural phase transformation.

2. Experimental

2.1. Synthesis

Crystals of $[C_6H_{16}N]_2[(UO_2)_6(MoO_4)_7(H_2O)_2](H_2O)_2$ were synthesized by a hydrothermal method from a solution of UO_2 $(CH_3COO)_2 \cdot 2H_2O$ (0.1568 g), MoO_3 (0.0576 g), triethylamine (0.054 g) and HCl (0.040 g) in 5 ml of H_2O (with an approximate U:Mo:triethylamine:HCl:H_2O molar gel ratio of 4:4:9:11:2780). The solution was placed in a Teflon-lined Parr bomb and heated to 180 °C for 43 h, followed by cooling to ambient temperature. The crystals occur as aggregates of yellow needles.

2.2. Single-crystal structure analysis

A crystal of $[C_6H_{16}N]_2[(UO_2)_6(MoO_4)_7(H_2O)_2](H_2O)_2$ was selected for X-ray data collection and mounted on a thin glass fiber. More than a hemisphere of X-ray diffraction data were collected at 20 °C using a Bruker SMART APEX CCD diffractometer with MoKα radiation. The data were integrated and corrected for absorption using an empirical ellipsoidal model supplied by the Bruker programs SAINT and XPREP. The absence conditions and reflection statistics indicated the orthorhombic space group $C222_1$, which was in agreement with previous studies of uranyl molybdates with $[(UO_2)_6(MoO_4)_7(H_2O)_2]$ frameworks [3,5]. The structure was solved by direct methods, yielding the positions of U, Mo and O atoms of the uranyl molybdate framework. Analysis of the difference Fourier maps revealed the presence of several partially-occupied positions in the framework cavities that can be assigned to disordered organic and H_2O molecules. Attempts to refine these positions were unsuccessful. Thus, they were introduced into the refinement, but their positional coordinates were not refined, whereas their isotropic thermal parameters were fixed at 0.15 Å^2; occupancies were fixed at the values corresponding to the heights of the residual peaks in the difference Fourier map. Later, the same crystal was measured at −127 °C using a Bruker SMART 1K CCD diffractometer with MoKα radiation. At this temperature, analysis of the diffraction pattern revealed the presence of several hundred relatively weak reflections that violate the $h + k = 2n$ absence conditions of the C-centered orthorhombic cell. The data were integrated and corrected for absorption using an empirical ellipsoidal model supplied by the Bruker programs SAINT and XPREP. The absence conditions and reflection statistics indicated the orthorhombic space group $P2_12_12_1$ which is a subgroup of the $C222_1$ space group found for the same crystal at room-temperature. The structure was solved by direct methods and refined in the space group $P2_12_12_1$ The refinement included not only the positions of U, Mo and O atoms of the uranyl molybdate framework, but also the positions of extra-framework protonated triethylamine molecules and H_2O groups (guest molecules).

Additional information pertinent to the data collections and structure refinements is given in Table 1. Atomic coordinates and displacement parameters for the structures at 20 and −127 °C are given in Tables 2 and 3, respectively. Selected bond-lengths for the structures at 20 and −127 °C are given in Tables 4 and 5, respectively. Table 6 provides values of the U–O–Mo bond angles for both temperatures studied.

The difference in symmetry of the structure at 20 and −127 °C provides evidence of a $C222_1 \rightarrow P2_12_12_1$ structural phase transition. To characterize the phase transition, the crystal was transferred to a CAD4 Enraf-Nonius four-circle single crystal diffractometer. A conventional liquid nitrogen device with an accuracy ±2 °C was

Table 1
Crystallographic data and refinement parameters for $[C_6H_{16}N]_2[(UO_2)_6(MoO_4)_7(H_2O)_2](H_2O)_2$ at 20 and −127 °C

	20 °C	−127 °C
a (Å)	11.3045(14)	11.211(4)
b (Å)	19.962(6)	19.880(10)
c (Å)	24.416(5)	24.421(8)
V (Å^3)	5510(2)	5443(4)
Space group	$C222_1$	$P2_12_12_1$
μ (cm^{-1})	192.90	194.33
Z	4	4
Diffractometer	SMART APEX CCD	SMART 1K CCD
Radiation	MoKα	MoKα
Total Ref.	31,126	31,610
Unique	11,422	12,009
Unique $\lvert F_o\rvert \geqslant 4\sigma_F$	6093	6951
R_1	0.046	0.047
wR_2	0.096	0.068
S	0.812	0.832

Note: $R_1 = \sum \lVert F_o\rvert - \lvert F_c\rVert / \sum \lvert F_o\rvert$; $wR_2 = \{\sum[w(F_o^2 - F_c^2)^2] / \sum[w(F_o^2)^2]\}^{1/2}$; $w = 1/[\sigma^2(F_o^2) + (aP^2 + bP)]$, where $P = (F_o^2 + 2F_c^2)/3$; $s = \{\sum[w(F_o^2 - F_c^2)]/(n-p)\}^{1/2}$ where n is the number of reflections and p is the number of refined parameters.

Table 2
Atomic coordinates and displacement parameters for $[C_6H_{16}N]_2[(UO_2)_6(MoO_4)_7(H_2O)_2](H_2O)_2$ at 20 °C

Atom	x	y	z	U_{eq}	U_{11}	U_{22}	U_{33}	U_{23}	U_{13}	U_{12}
U(1)	0.45617(5)	0.24441(3)	−0.01695(2)	0.0206(1)	0.0204(3)	0.0230(3)	0.0185(2)	−0.0005(2)	−0.0012(2)	−0.0033(2)
U(2)	0.39919(6)	0.47339(3)	0.38411(2)	0.0205(1)	0.0270(3)	0.0169(3)	0.0177(3)	−0.0022(2)	0.0046(2)	−0.0023(2)
U(3)	0.75723(6)	0.24510(4)	0.25615(2)	0.0297(2)	0.0332(4)	0.0373(4)	0.0186(3)	−0.0032(3)	−0.0029(3)	0.0161(3)
Mo(1)	0.5000	0.38523(9)	0.2500	0.0212(4)	0.0270(11)	0.0155(8)	0.0210(9)	0.000	0.0061(8)	0.000
Mo(2)	0.99053(13)	0.15503(6)	0.15950(5)	0.0199(3)	0.0259(7)	0.0187(6)	0.0150(6)	−0.0015(5)	−0.0016(5)	0.0023(6)
Mo(3)	0.65611(12)	0.27664(6)	0.10346(5)	0.0184(3)	0.0200(7)	0.0181(6)	0.0171(6)	−0.0014(5)	−0.0011(5)	0.0017(5)
Mo(4)	0.22207(12)	0.11655(6)	0.01626(6)	0.0191(3)	0.0202(7)	0.0168(6)	0.0203(6)	0.0006(5)	0.0007(5)	−0.0024(5)
O(1)	0.2741(12)	0.4710(7)	0.3395(5)	0.041(3)	0.039(8)	0.057(9)	0.028(6)	−0.016(7)	0.009(6)	−0.009(7)
O(2)	0.8765(12)	0.1683(6)	0.2068(4)	0.037(3)	0.056(9)	0.043(8)	0.011(5)	0.002(5)	0.007(5)	0.028(7)
O(3)	0.9426(11)	0.1834(6)	0.0978(5)	0.035(3)	0.032(7)	0.039(7)	0.036(7)	0.014(6)	0.005(6)	0.003(6)
O(4)	0.3626(11)	0.2994(7)	0.0213(5)	0.035(3)	0.037(8)	0.049(8)	0.019(6)	0.007(6)	−0.010(5)	−0.010(6)
O(5)	0.6841(10)	0.2377(6)	0.1672(4)	0.028(3)	0.037(7)	0.029(6)	0.019(5)	0.001(5)	−0.010(5)	0.010(6)
O(6)	0.0161(14)	0.0700(6)	0.1600(5)	0.041(3)	0.062(10)	0.030(7)	0.030(7)	−0.002(5)	0.011(7)	0.009(7)
O(7)	0.2189(12)	0.0648(6)	−0.0419(5)	0.036(3)	0.037(8)	0.033(7)	0.037(7)	−0.014(6)	0.005(6)	−0.018(6)
O(8)	0.6475(13)	0.1852(8)	0.2730(6)	0.059(5)	0.041(10)	0.089(13)	0.046(9)	0.042(8)	0.011(7)	0.010(8)
O(9)	0.8654(14)	0.3059(8)	0.2400(7)	0.060(4)	0.045(10)	0.059(10)	0.075(12)	−0.006(9)	−0.018(8)	0.013(8)
O(10)	0.8795(15)	0.1979(8)	0.3210(5)	0.059(5)	0.072(12)	0.081(11)	0.026(7)	0.008(7)	−0.023(7)	0.033(9)
O(11)	0.5602(10)	0.2253(6)	0.0674(5)	0.031(3)	0.026(7)	0.033(7)	0.034(6)	−0.001(5)	−0.011(5)	−0.012(5)
O(12)	0.6233(16)	0.3342(7)	0.2479(6)	0.063(5)	0.095(14)	0.061(10)	0.032(7)	−0.012(8)	0.013(8)	0.042(9)
O(13)	0.5129(12)	0.4358(6)	0.3066(5)	0.035(3)	0.049(9)	0.028(6)	0.028(6)	−0.004(5)	0.008(6)	−0.010(6)
O(14)	0.1857(13)	0.0684(6)	0.0757(5)	0.040(3)	0.048(9)	0.025(7)	0.047(8)	−0.001(6)	0.008(7)	0.000(6)
O(15)	0.5894(10)	0.3526(5)	0.1174(5)	0.026(2)	0.024(6)	0.022(5)	0.033(6)	0.003(5)	0.001(5)	0.001(5)
O(16)	0.5266(11)	0.4751(7)	0.4256(5)	0.038(3)	0.036(8)	0.045(7)	0.032(7)	−0.007(6)	−0.008(6)	0.004(6)
O(17)	0.3665(11)	0.1511(6)	0.0267(5)	0.034(3)	0.027(7)	0.041(7)	0.034(7)	0.013(6)	−0.005(5)	−0.011(6)
O(18)	0.6102(12)	0.3224(6)	−0.0098(6)	0.042(3)	0.050(9)	0.025(6)	0.052(8)	0.011(6)	−0.013(7)	−0.016(6)
O(19)	0.5484(11)	0.1915(6)	−0.0563(5)	0.035(3)	0.029(7)	0.045(8)	0.030(6)	−0.006(6)	0.009(6)	−0.012(6)
O(20)	0.7926(11)	0.2910(6)	0.0730(5)	0.036(3)	0.031(8)	0.043(8)	0.035(7)	−0.006(6)	−0.006(6)	0.001(6)
H_2O(21)	0.711(3)	0.2913(11)	0.3479(6)	0.133(11)	0.24(3)	0.133(19)	0.028(9)	0.008(10)	0.036(13)	0.113(19)

Peaks in the difference Fourier map

Q(1)	4.00 e^-	0.8777	0.5153	0.3632	0.15[a]
Q(2)	3.28e^-	0.7475	0.3996	0.4122	0.15[a]
Q(3)	2.32e^-	0.8799	0.5509	0.3207	0.15[a]
Q(4)	1.52e^-	0.7688	0.5778	0.4345	0.15[a]
Q(5)	2.16e^-	0.9669	0.5267	0.3709	0.15[a]
Q(6)	2.08e^-	0.7805	0.5256	0.2831	0.15[a]
Q(7)	2.00e^-	0.0253	0.5906	0.3590	0.15[a]
Q(8)	1.76e^-	0.0233	0.4115	0.3484	0.15[a]

[a] Fixed during refinement.

used to control the temperature. The unit-cell parameters were measured at 20, 0, −18, −65, −72, −92, −115 and −147 °C. The intensities of reflections allowed for $P2_12_12_1$ but forbidden for $C222_1$ (810, 41.10 and 650) as well as intensities of reflections allowed for both space groups (730, 177 and 609) were monitored as a function of temperature. It is interesting that the unit-cell parameters of $[C_6H_{16}N]_2[(UO_2)_6(MoO_4)_7(H_2O)_2](H_2O)_2$ measured at room temperature one hour after cooling [a = 11.271(2), b = 19.969(4), c = 24.345(3) Å, V = 5479(2) Å^3] are not the same as they are at the room temperature before cooling (Table 1). However, the unit-cell parameters measured one week after the low-temperature experiment more or less return to their original values [a = 11.298(1), b = 19.962(4), c = 24.411(3) Å, V = 5505(2) Å^3]. This shows that the structure possess some memory of its temperature history.

2.3. X-ray powder-diffraction study

X-ray powder-diffraction pattern of $[C_6H_{16}N]_2[(UO_2)_6(MoO_4)_7(H_2O)_2](H_2O)_2$ was recorded at room temperature using a DRON-2 powder diffractometer and CuKα radiation (λ = 1.54059 Å). The unit-cell parameters refined from powder data using least-squares methods and 60 reflections are: a = 11.3227(8), b = 20.004(1), c = 24.456(2) Å. These parameters and the experimental diffraction pattern are in reasonably good agreement with the results of single-crystal diffraction analysis.

High-temperature X-ray powder diffraction study was performed in the range of temperatures from 20 to 700 °C by means of a DRON-3 powder diffractometer equipped with a high-temperature KRV-1100 chamber. The phase is stable until 270 ± 10 °C. In between 300

Table 3
Atomic coordinates and displacement parameters for $[C_6H_{16}N]_2[(UO_2)_6(MoO_4)_7(H_2O)_2](H_2O)_2$ at −127 °C

Atom	*x*	*y*	*z*	U_{eq}
U(1A)	0.20986(6)	0.75745(4)	0.02001(3)	0.0151(2)
U(1B)	0.70691(6)	0.25891(4)	0.01639(3)	0.0147(2)
U(2A)	0.34056(6)	0.52845(4)	−0.11363(3)	0.0147(2)
U(2B)	0.35406(6)	0.47421(4)	0.11741(3)	0.0153(2)
U(3A)	0.02448(6)	0.24524(3)	−0.25562(4)	0.0213(2)
U(3B)	0.00942(6)	0.23782(4)	0.24335(4)	0.0216(2)
Mo(1)	0.25671(14)	0.38728(6)	0.24999(11)	0.0150(3)
Mo(2A)	0.23264(15)	0.65646(11)	0.15988(8)	0.0132(5)
Mo(2B)	0.24735(13)	0.34460(12)	−0.15935(9)	0.0151(5)
Mo(3A)	−0.09530(13)	0.77601(9)	0.10208(7)	0.0129(4)
Mo(3B)	−0.09310(14)	0.22206(8)	−0.10394(7)	0.0138(4)
Mo(4A)	0.47620(14)	0.61617(7)	0.01777(7)	0.0139(4)
Mo(4B)	0.46807(15)	0.38321(8)	−0.01604(7)	0.0149(4)
O(1A)	0.4655(11)	0.5314(6)	−0.1557(6)	0.024(3)
O(1B)	0.4792(10)	0.4687(6)	0.1587(5)	0.019(3)
O(2A)	0.1438(11)	0.3265(6)	−0.2093(6)	0.024(3)
O(2B)	0.1148(11)	0.6628(7)	0.2071(6)	0.024(3)
O(3A)	0.1828(11)	0.6814(6)	0.0957(6)	0.024(3)
O(3B)	0.2031(11)	0.3090(6)	−0.0981(5)	0.022(3)
O(4A)	0.3009(12)	0.8081(7)	0.0602(6)	0.029(4)
O(4B)	0.6141(11)	0.2017(6)	−0.0172(6)	0.024(4)
O(5A)	−0.0574(10)	0.2595(6)	−0.1664(5)	0.021(3)
O(5B)	−0.0720(10)	0.7361(6)	0.1649(5)	0.021(3)
O(6A)	0.2541(10)	0.4331(7)	−0.1539(6)	0.024(4)
O(6B)	0.2821(12)	0.5745(7)	0.1588(6)	0.023(3)
O(7A)	0.4635(11)	0.5642(6)	−0.0403(5)	0.019(3)
O(7B)	0.4670(12)	0.4350(6)	0.0419(6)	0.023(3)
O(8A)	0.1312(11)	0.1875(6)	−0.2348(6)	0.030(4)
O(8B)	0.1190(11)	0.1774(6)	0.2314(5)	0.029(4)
O(9A)	−0.0827(9)	0.3023(5)	−0.2770(6)	0.037(4)
O(9B)	−0.0991(8)	0.2980(5)	0.2547(7)	0.036(4)
O(10A)	0.3473(12)	0.7105(7)	0.1792(6)	0.033(4)
O(10B)	0.3861(11)	0.3125(6)	−0.1777(6)	0.030(4)
O(11A)	−0.1799(10)	0.7207(6)	0.0610(5)	0.018(3)
O(11B)	−0.1886(11)	0.2750(7)	−0.0669(5)	0.024(3)
O(12A)	0.3878(11)	0.3419(6)	0.2442(7)	0.033(3)
O(12B)	0.1387(11)	0.3316(6)	0.2527(7)	0.037(4)
O(13A)	0.2718(11)	0.4360(7)	0.3103(6)	0.019(3)
O(13B)	0.2390(10)	0.4376(8)	0.1931(6)	0.019(4)
O(14A)	0.4256(11)	0.4301(7)	−0.0725(6)	0.025(4)
O(14B)	0.4467(10)	0.5671(6)	0.0759(5)	0.015(3)
O(15A)	−0.1716(10)	0.8504(6)	0.1131(6)	0.018(3)
O(15B)	−0.1629(10)	0.1448(6)	−0.1154(6)	0.021(3)
O(16A)	0.2158(11)	0.5278(7)	−0.0700(6)	0.018(3)
O(16B)	0.2285(11)	0.4770(8)	0.0752(6)	0.024(3)
O(17A)	0.6219(10)	0.6474(6)	0.0226(5)	0.016(3)
O(17B)	0.6092(11)	0.3486(6)	−0.0301(5)	0.024(3)
O(18 A)	0.3692(11)	0.6801(6)	0.0147(6)	0.027(4)
O(18B)	0.3607(11)	0.3212(6)	−0.0081(6)	0.027(4)
O(19A)	0.1163(11)	0.7063(7)	−0.0181(6)	0.027(4)
O(19B)	0.8039(11)	0.3158(6)	0.0497(6)	0.022(3)
O(20A)	0.0448(11)	0.7940(6)	0.0717(5)	0.021(3)
O(20B)	0.0409(11)	0.2082(6)	−0.0680(5)	0.018(3)
H_2O(21A)	0.0695(12)	0.2819(7)	0.1500(6)	0.046(4)
H_2O(21B)	−0.0004(13)	0.1867(7)	−0.3491(7)	0.057(5)
Extra-framework positions				
H_2O(22)	0.0025(12)	0.3938(7)	0.0903(6)	0.042(4)
H_2O(23)	−0.2467(19)	0.6069(11)	−0.1689(9)	0.105(8)
N(1)	−0.1499(15)	0.4839(9)	−0.1392(7)	0.049(3)[a]
C(1)	−0.2528(17)	0.4573(11)	−0.1055(9)	0.049(3)[a]
C(2)	−0.274(2)	0.5001(11)	−0.0552(9)	0.049(3)[a]
C(3)	−0.0443(18)	0.4877(10)	−0.1047(9)	0.049(3)[a]

Table 3 (*continued*)

Atom	*x*	*y*	*z*	U_{eq}
C(4)	−0.013(2)	0.4241(11)	−0.0719(10)	0.049(3)[a]
C(5)	−0.1290(19)	0.4353(11)	−0.1872(8)	0.049(3)[a]
C(6)	−0.0384(19)	0.4623(11)	−0.2262(9)	0.049(3)[a]
N(2)	−0.1079(16)	0.5183(10)	0.1300(8)	0.060(3)[a]
C(7)	−0.2398(17)	0.5243(12)	0.1236(11)	0.060(3)[a]
C(8)	−0.279(2)	0.5916(11)	0.1473(11)	0.060(3)[a]
C(9)	−0.058(2)	0.5170(11)	0.1891(9)	0.060(3)[a]
C(10)	−0.116(2)	0.4602(11)	0.2199(10)	0.060(3)[a]
C(11)	−0.033(2)	0.5712(11)	0.0989(9)	0.060(3)[a]
C(12)	−0.049(2)	0.5696(12)	0.0373(9)	0.060(3)[a]

Atom	U_{11}	U_{22}	U_{33}	U_{23}	U_{13}	U_{12}
U(1A)	0.0164(3)	0.0166(5)	0.0124(5)	0.0008(4)	0.0017(3)	0.0011(4)
U(1B)	0.0164(3)	0.0163(4)	0.0115(5)	−0.0011(4)	0.0001(3)	0.0004(4)
U(2A)	0.0192(4)	0.0132(4)	0.0118(5)	0.0011(4)	−0.0027(3)	−0.0012(3)
U(2B)	0.0211(4)	0.0132(4)	0.0115(5)	0.0014(4)	0.0032(3)	0.0028(3)
U(3A)	0.0256(3)	0.0263(4)	0.0121(5)	−0.0018(4)	0.0022(4)	−0.0121(4)
U(3B)	0.0237(4)	0.0285(4)	0.0126(5)	0.0024(4)	−0.0027(3)	−0.0115(4)
Mo(1)	0.0212(7)	0.0125(7)	0.0113(8)	0.0003(12)	0.0028(7)	0.0007(7)
Mo(2A)	0.0177(9)	0.0106(12)	0.0114(11)	−0.0003(9)	0.0004(8)	−0.0002(7)
Mo(2B)	0.0213(10)	0.0147(13)	0.0092(11)	0.0000(9)	0.0011(7)	−0.0010(7)
Mo(3A)	0.0148(8)	0.0148(10)	0.0092(10)	0.0003(8)	−0.0006(7)	0.0007(7)
Mo(3B)	0.0162(8)	0.0131(10)	0.0122(11)	−0.0011(8)	−0.0004(7)	0.0004(7)
Mo(4A)	0.0163(7)	0.0130(8)	0.0124(11)	0.0004(7)	−0.0001(8)	0.0016(7)
Mo(4B)	0.0179(8)	0.0146(9)	0.0122(11)	0.0001(8)	−0.0026(8)	0.0027(7)

[a] Constrained to be equal during refinement.

Table 4
Selected bond lengths (Å) in the structure of $[C_6H_{16}N]_2[(UO_2)_6(MoO_4)_7(H_2O)_2](H_2O)_2$ at 20 °C

U(1)–O(19)	1.77(1)	Mo(1)–O(13)	1.72(1) 2*x*
U(1)–O(4)	1.79(1)	Mo(1)–O(12)	1.73(2) 2*x*
U(1)–O(18)	2.34(1)	⟨Mo(1)–O⟩	
U(1)–O(17)	2.37(1)		
U(1)–O(11)	2.40(1)	Mo(2)–O(3)	1.70(1)
U(1)–O(20)	2.41(1)	Mo(2)–O(6)	1.72(1)
U(1)–O(3)	2.45(1)	Mo(2)–O(2)	1.75(1)
⟨U(1)–O_{Ur}⟩		Mo(2)–O(10)	1.77(1)
⟨U(1)–O_{eq}⟩		⟨Mo(2)–O⟩	
U(2)–O(16)	1.76(1)	Mo(3)–O(15)	1.73(1)
U(2)–O(1)	1.79(1)	Mo(3)–O(11)	1.73(1)
U(2)–O(14)	2.34(1)	Mo(3)–O(20)	1.74(1)
U(2)–O(7)	2.37(1)	Mo(3)–O(5)	1.77(1)
U(2)–O(13)	2.41(1)	⟨Mo(3)–O⟩	
U(2)–O(6)	2.41(1)		
U(2)–O(15)	2.42(1)	Mo(4)–O(7)	1.76(1)
⟨U(2)–O_{Ur}⟩		Mo(4)–O(18)	1.76(1)
⟨U(2)–O_{eq}⟩		Mo(4)–O(14)	1.79(1)
		Mo(4)–O(17)	1.79(1)
U(3)–O(9)	1.77(2)	⟨Mo(4)–O⟩	
U(3)–O(8)	1.77(2)		
U(3)–O(10)	2.30(1)		
U(3)–O(5)	2.33(1)		
U(3)–O(12)	2.34(1)		
U(3)–O(2)	2.37(1)		
U(3)–O(21)	2.48(2)		
⟨U(3)–O_{Ur}⟩			
⟨U(3)–O_{eq}⟩			

and 500 °C, no diffraction peaks are observed. At 500 ± 10 °C, the compound UO_2MoO_4 crystallizes.

3. Results and discussion

The structure of $[C_6H_{16}N]_2[(UO_2)_6(MoO_4)_7(H_2O)_2](H_2O)_2$ is based upon the U:Mo = 6:7 framework consisting of corner-sharing UO_7 pentagonal bipyramids and MoO_4 tetrahedra. The chiral framework channels along the *c*-axis are filled by guest molecules: extra-framework H_2O groups and protonated triethylamine molecules (Figs. 1 and 2), ordered at low temperatures and disordered at ambient conditions. The ordered state corresponds to the lower symmetry. The observed symmetry reduction implies that an order parameter (OP, η) for the structural phase transition $C222_1 \rightarrow P2_12_12_1$ transforms according to the irreducible representation Y_2 of the space group $C222_1$ [6]. Such a transition may (by symmetry) be of second order and the free energy series expansion (Landau potential) can be expressed as a sum of even orders of OP. Truncation of the Landau potential after the fourth order term leads to the well-known equation for temperature dependence of the square of the order parameter $\eta^2 = -\frac{\alpha}{\beta}(T - T_c)$ [7], where T_c is the temperature of the transition, α and β are phenomenological coefficients. The unit cell volume as a function of temperature (Fig. 3) does not show any response to the

Table 5
Selected bond lengths (Å) in the structure of $[C_6H_{16}N]_2[(UO_2)_6(MoO_4)_7(H_2O)_2](H_2O)_2$ at −127 °C

U(1A)–O(19A)	1.73(1)	U(3A)–O(9A)	1.733(5)	Mo(3A)–O(15A)	1.73(1)
U(1A)–O(4A)	1.74(1)	U(3A)–O(8A)	1.73(1)	Mo(3A)–O(5B)	1.75(1)
U(1A)–O(20A)	2.36(1)	U(3A)–O(10A)	2.32(1)	Mo(3A)–O(11A)	1.77(1)
U(1A)–O(18A)	2.36(1)	U(3A)–O(12A)	2.33(1)	Mo(3A)–O(20A)	1.77(1)
U(1A)–O(17A)	2.37(1)	U(3A)–O(5A)	2.38(1)	⟨Mo(3A)–O⟩	1.76
U(1A)–O(11A)	2.37(1)	U(3A)–O(2A)	2.38(1)		
U(1A)–O(3A)	2.41(1)	U(3A)–O(21A)	2.58(2)	Mo(3B)–O(5A)	1.74(1)
⟨U(1A)–O_{Ur}⟩	1.74	⟨U(3A)–O_{Ur}⟩	1.73	Mo(3B)–O(15B)	1.75(1)
⟨U(1A)–O_{eq}⟩	2.37	⟨U(3A)–O_{eq}⟩	2.40	Mo(3B)–O(11B)	1.75(1)
				Mo(3B)–O(20B)	1.76(1)
U(1B)–O(4B)	1.75(1)	U(3B)–O(9B)	1.729(5)	⟨Mo(3B)–O⟩	1.75
U(1B)–O(19B)	1.77(1)	U(3B)–O(8B)	1.74(1)		
U(1B)–O(20B)	2.34(1)	U(3B)–O(10B)	2.34(1)	Mo(4A)–O(18A)	1.75(1)
U(1B)–O(18B)	2.36(1)	U(3B)–O(5B)	2.35(1)	Mo(4A)–O(17A)	1.75(1)
U(1B)–O(11B)	2.37(1)	U(3B)–O(2B)	2.37(1)	Mo(4A)–O(14B)	1.75(1)
U(1B)–O(17B)	2.38(1)	U(3B)–O(12B)	2.37(1)	Mo(4A)–O(7A)	1.76(1)
U(1B)–O(3B)	2.41(1)	U(3B)–O(21B)	2.53(2)	⟨Mo(4A)–O⟩	1.75
⟨U(1B)–O_{Ur}⟩	1.76	⟨U(3B)–O_{Ur}⟩	1.73		
⟨U(1B)–O_{eq}⟩	2.37	⟨U(3B)–O_{eq}⟩	2.39	Mo(4B)–O(14A)	1.73(1)
				Mo(4B)–O(18B)	1.73(1)
U(2A)–O(1A)	1.74(1)	Mo(1)–O(13B)	1.72(2)	Mo(4B)–O(7B)	1.75(1)
U(2A)–O(16A)	1.76(1)	Mo(1)–O(12B)	1.73(1)	Mo(4B)–O(17B)	1.76(1)
U(2A)–O(6A)	2.35(1)	Mo(1)–O(12A)	1.73(1)	⟨Mo(4B)–O⟩	1.74
U(2A)–O(13A)	2.35(1)	Mo(1)–O(13A)	1.77(1)		
U(2A)–O(7A)	2.37(1)	⟨Mo(1)–O⟩	1.74	N(1)–C(3)	1.46(2)
U(2A)–O(14A)	2.40(1)			N(1)–C(1)	1.51(2)
U(2A)–O(15A)	2.41(1)	Mo(2A)–O(6B)	1.72(1)	N(1)–C(5)	1.54(2)
⟨U(2A)–O_{Ur}⟩	1.75	Mo(2A)–O(3A)	1.74(1)	C(1)–C(2)	1.51(2)
⟨U(2A)–O_{eq}⟩	2.37	Mo(2A)–O(10A)	1.74(1)	C(3)–C(4)	1.54(2)
		Mo(2A)–O(2B)	1.76(1)	C(5)–C(6)	1.49(2)
U(2B)–O(1B)	1.73(1)	⟨Mo(2A)–O⟩	1.74	N(2)–C(7)	1.49(2)
U(2B)–O(16B)	1.75(1)			N(2)–C(11)	1.55(2)
U(2B)–O(14B)	2.35(1)	Mo(2B)–O(2A)	1.72(1)	N(2)–C(9)	1.55(2)
U(2B)–O(7B)	2.37(1)	Mo(2B)–O(3B)	1.73(1)	C(7)–C(8)	1.52(2)
U(2B)–O(13B)	2.37(1)	Mo(2B)–O(10B)	1.74(1)	C(9)–C(10)	1.51(2)
U(2B)–O(15B)	2.37(1)	Mo(2B)–O(6A)	1.77(2)	C(11)–C(12)	1.52(2)
U(2B)–O(6B)	2.38(1)	⟨Mo(2B)–O⟩	1.75		
⟨U(2B)–O_{Ur}⟩	1.74				
⟨U(2B)–O_{eq}⟩	2.37				

phase transition, thus indicating its second-order character. The temperature dependence of the individual cell dimensions is more complicated: whereas *a* and *b* show more or less linear behavior, the *c* parameter deviates from linear behavior close to the transition temperature and increases with cooling. Keeping in mind that the chiral channels propagate along the *c*-axis, the length of the spiral-like channels must increase over the phase transition.

The intensities of superstructure reflections as a measure of deviation from $C222_1$ symmetry are proportional to the square of OP and thus should exhibit linear temperature dependence in the neighborhood of the transition temperature. Fig. 4 shows the intensities of selected reflections versus temperature. The intensities of reflections that should be absent in the *C*-centered high-temperature structure (810, 650, 41.10) appear at temperatures of ~−10 °C and increase in intensity with decreasing temperature. Intensities of the reflections that are present in both $C222_1$ and $P2_12_12_1$ structures (730, 177, 609) increase (609) or decrease (730) with temperature or remain more or less constant within the temperature range of −147 to +20 °C. A linear fit of the temperature dependence of normalized intensities for the *C*-violating reflections allows an estimation of the temperature of the $C222_1 \rightarrow P2_12_12_1$ phase transition at −11(5) °C (Fig. 5).

The significant difference between the high-temperature $C222_1$ and low-temperature $P2_12_12_1$ structures is in the degree of ordering of guest molecules and in the deformation of the flexible framework in order to adopt to this ordering. In the $C222_1$ structure at 20 °C, H_2O and $[C_6H_{16}N]^+$ molecules are disordered, whereas, in the $P2_12_12_1$ structure at −127 °C, they are perfectly ordered. The latter structure contains two symmetrically independent $[C_6H_{16}N]^+$ molecules and two symmetri-

Table 6
Values of the U–O_{br}–Mo angles (O_{br} = bridging O atom) in the structure of $[C_6H_{16}N]_2[(UO_2)_6(MoO_4)_7(H_2O)_2](H_2O)_2$ above (20 °C) and below (−127 °C) phase transition

U–O–Mo angles at 20 °C		U–O–Mo angles at −127 °C		Δ
U(3)–O(2)–Mo(2)	148.4(7)	U(3A)–O(2A)–Mo(2B)	149.0(7)	3.9
		U(3B)–O(2B)–Mo(2A)	145.1(7)	
U(1)–O(3)–Mo(2)	153.1(7)	U(1A)–O(3A)–Mo(2A)	146.3(7)	**14.0**
		U(1B)–O(3B)–Mo(2B)	160.3(7)	
U(3)–O(5)–Mo(3)	148.9(6)	U(3A)–O(5A)–Mo(3B)	146.9(7)	4.2
		U(3B)–O(5B)–Mo(3A)	151.1(7)	
U(2)–O(6)–Mo(2)	148.6(7)	U(2A)–O(6A)–Mo(2B)	148.7(7)	4.8
		U(2B)–O(6B)–Mo(2A)	155.5(8)	
U(2)–O(7)–Mo(4)	144.7(7)	U(2A)–O(7A)–Mo(4A)	146.3(7)	0.6
		U(2B)–O(7B)–Mo(4B)	145.7(7)	
U(3)–O(10)–Mo(2)	152.0(8)	U(3A)–O(10A)–Mo(2A)	151.5(8)	2.1
		U(3B)–O(10B)–Mo(2B)	149.4(8)	
U(1)–O(11)–Mo(3)	130.4(6)	U(1A)–O(11A)–Mo(3A)	129.8(6)	1.8
		U(1B)–O(11B)–Mo(3B)	131.6(7)	
U(3)–O(12)–Mo(1)	165.0(10)	U(3A)–O(12A)–Mo(1)	159.5(8)	6.0
		U(3B)–O(12B)–Mo(1)	165.5(8)	
U(2)–O(13)–Mo(1)	140.4(7)	U(2A)–O(13A)–Mo(1)	140.3(7)	2.2
		U(2B)–O(13B)–Mo(1)	138.1(6)	
U(2)–O(14)–Mo(4)	150.4(7)	U(2A)–O(14A)–Mo(4B)	151.9(8)	1.5
		U(2B)–O(14B)–Mo(4A)	150.4(7)	
U(2)–O(15)–Mo(3)	148.2(6)	U(2A)–O(15A)–Mo(3A)	145.7(6)	1.9
		U(2B)–O(15B)–Mo(3B)	147.6(6)	
U(1)–O(17)–Mo(4)	128.9(6)	U(1A)–O(17A)–Mo(4A)	129.9(6)	2.1
		U(1B)–O(17B)–Mo(4B)	127.8(7)	
U(1)–O(18)–Mo(4)	170.3(8)	U(1A)–O(18A)–Mo(4A)	171.9(8)	3.6
		U(1B)–O(18B)–Mo(4B)	168.3(9)	
U(1)–O(20)–Mo(3)	151.4(7)	U(1A)–O(20A)–Mo(3A)	149.1(7)	5.4
		U(1B)–O(20B)–Mo(3B)	154.5(6)	

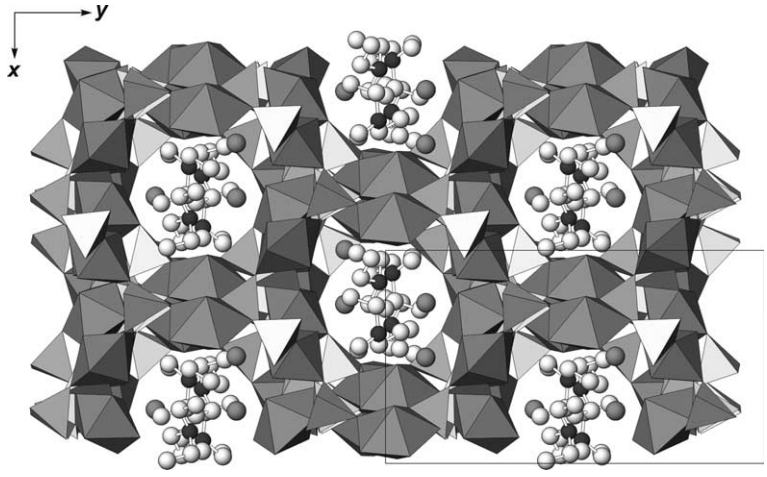

Fig. 1. The crystal structure of $[C_6H_{16}N]_2[(UO_2)_6(MoO_4)_7(H_2O)_2](H_2O)_2$ at −127 °C viewed along the *c*-axis. Legend: small dark grey circles = *N* atoms, small white circles = C atoms; large dark-grey circles = H_2O groups.

cally independent non-framework H_2O groups. As can be derived from the $N \cdots H_2O$ distances, there is a relatively strong $N–H \cdots H_2O$ hydrogen bond between each $[C_6H_{16}N]^+$ molecule and the adjacent H_2O group (Fig. 2a, b). With decreasing temperature each $[C_6H_{16}N]^+$ molecule in the framework channels (Fig. 2d) takes on one of the two orientations. These orientations are non-equivalent relative to the *C*-translation present in the $C222_1$ space group (Fig. 2c). Due to the interactions between framework and guest molecules

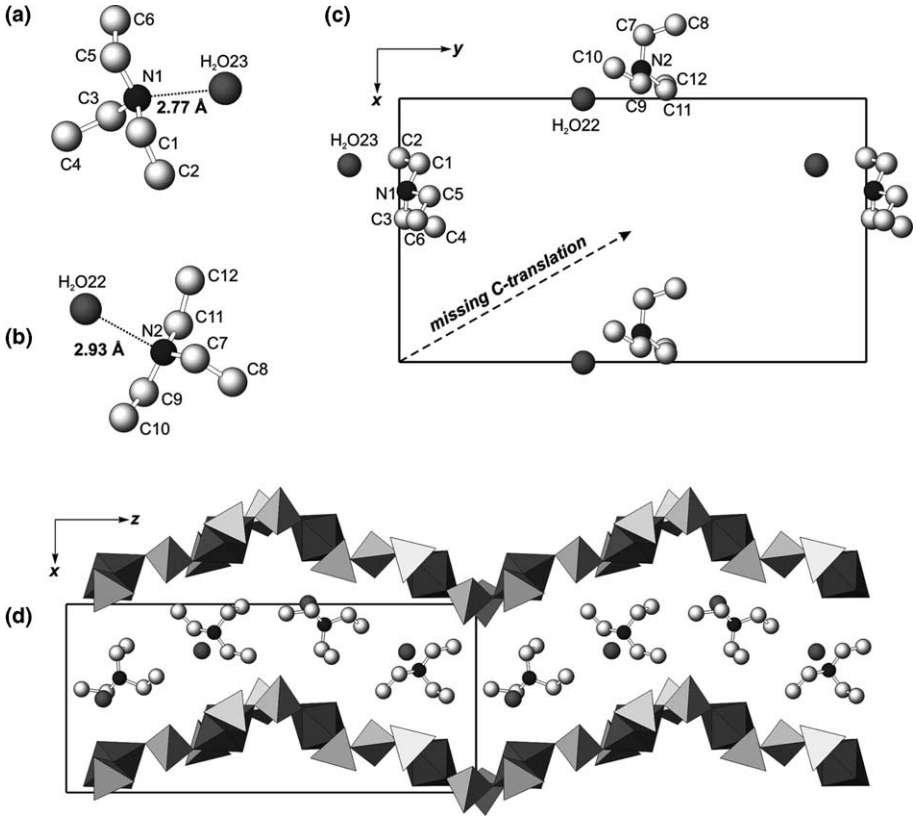

Fig. 2. Configurations of the two non-equivalent $[C_6H_{16}N]^+$ cations and adjacent H_2O groups (a,b), arrangement of extra-framework $[C_6H_{16}N]^+$ cations and H_2O groups located at $z \sim 0$ within the xy plane (c) and cross-section of the wave-like channel in the uranyl molybdate framework occupied by $[C_6H_{16}N]^+$ cations and H_2O groups (d). All diagrams are based upon −127 °C data. Legend as in Fig. 1.

the framework also losses its *C*-translational symmetry. From the crystallographic viewpoint, the $C222_1 \rightarrow P2_12_12_1$ phase transition corresponds to the splitting of each of the $C222_1$ atomic positions (except Mo(1)) into two, labeled as A and B in Tables 3, 5 and 6. Consequently, each of the U–O(*n*)–Mo angles in the high-temperature structure splits into two non-equivalent angles in the low-temperature structure, U–O(*n*A)–Mo and U–O(*n*B)–Mo. The difference Δ between the U–O(*n*A)–Mo and U–O(*n*B)–Mo angles reflects response of the framework to the ordering of molecules in the channels.

The most dramatic change is observed for the U(1A)–O(3A)–Mo(2A) and U(1B)–O(3B)–Mo(2B) angles for which the value of Δ equals 14.0°. This value corresponds to shifts of the heavy framework atoms from their positions in the high symmetry structure and provides the main contribution to the superstructure intensities measured by the X-ray diffraction. Together with the pronounced change in the *c* dimension, it can be recognized as a main indicator of the phase transition and can be monitored in the course of a more detailed structural study.

The remnant elastic strain and very long relaxation time discovered for the $C222_1 \rightarrow P2_12_12_1$ transformation on heating is quite unusual and may indicate the possible appearance of antiphase domains on the mesoscopic scale. However, more detailed investigation of this effect is needed in order to confirm this hypothesis.

4. Conclusions

In this contribution we report the new type of chiral open framework found in $[C_6H_{16}N]_2[(UO_2)_6(MoO_4)_7(H_2O)_2](H_2O)_2$ compound. The structure was studied by multi-temperature single-crystal X-ray diffraction. The second-order structural phase transition at −11 °C has been described as associated with the ordering of guest molecules and corresponding distortions of the flexible uranyl molybdate framework. Both processes lead to the loss of the *C*-centering and corresponding change of the space group from $C222_1$ to $P2_12_12_1$ and thus contribute to the same order parameter spanning the Y_2 irreducible representation.

The examples of uranyl molybdate frameworks considered before [1–3] highlight the flexibility of the structure adopting guests of different chemistry and of

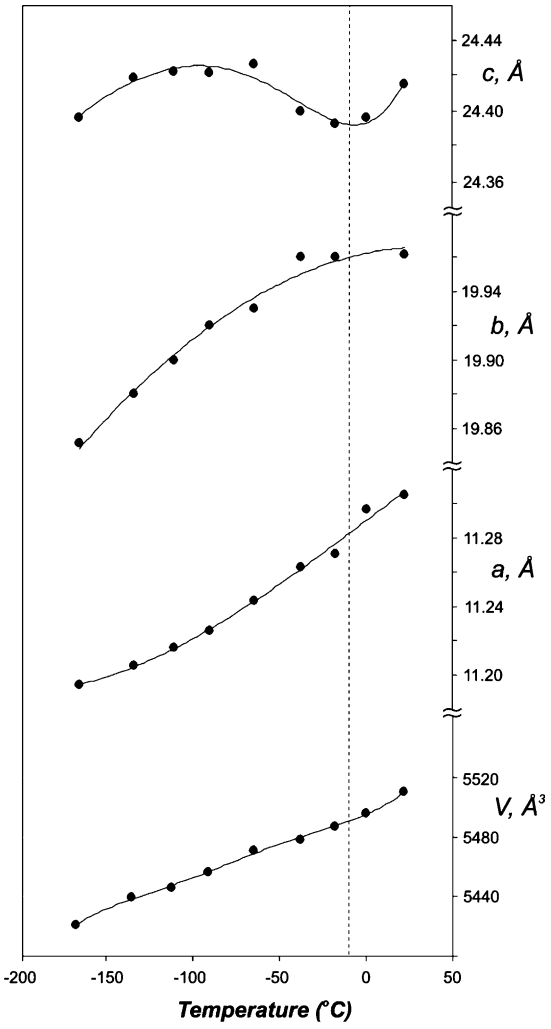

Fig. 3. Unit-cell parameters and unit-cell volume of $[C_6H_{16}N]_2$-$[(UO_2)_6(MoO_4)_7(H_2O)_2](H_2O)_2$ versus temperature.

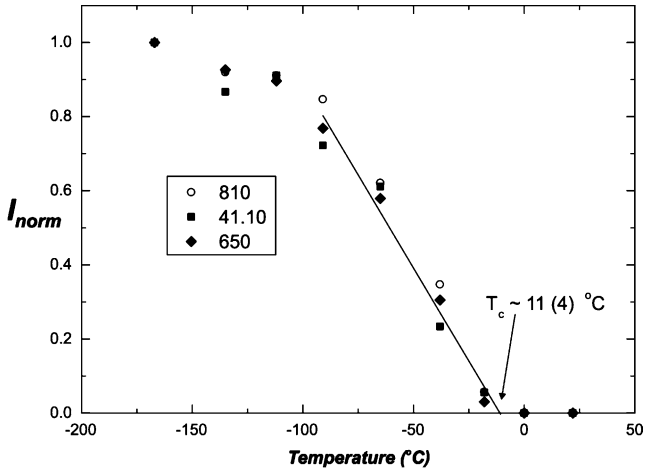

Fig. 5. Normalized intensities of the *C*-translation-violating reflections versus temperature. Intersection of the linear fit of the last four points with the *x*-axis gives the temperature of the phase transition.

various geometric shape. In the structural realization considered here the framework demonstrates its high flexibility by adopting different degrees of ordering of the guest molecules.

Acknowledgments

This research was supported by the Environmental Management Sciences Program of the United States Department of Energy (Grant DE-FG07-97ER14820). S.V.K. thanks Alexander von Humboldt Foundation and Swiss National Foundation for financial support during his stay at Bern.

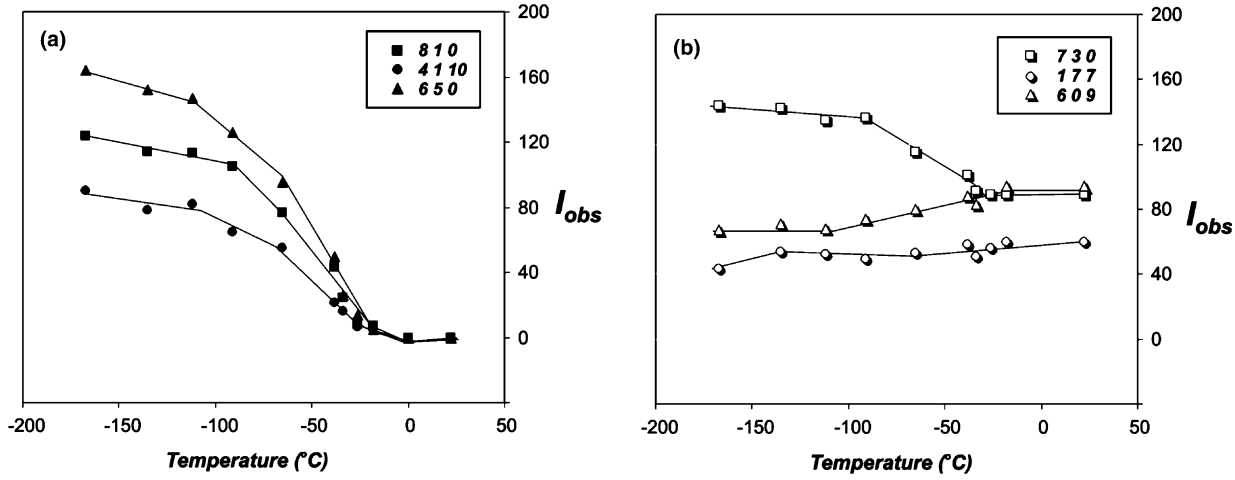

Fig. 4. Intensities of *C*-translation-violating (a) and non-violating (b) reflections versus temperature.

References

[1] S.V. Krivovichev, C.L. Cahill, P.C. Burns, Inorg. Chem. 42 (2003) 2459.
[2] S.V. Krivovichev, C.L. Cahill, E.V. Nazarchuk, P.C. Burns, T. Armbruster, W. Depmeier, Micropor. Mesopor. Mater. 78 (2005) 209.
[3] S.V. Krivovichev, P.C. Burns, T. Armbruster, E.V. Nazarchuk, W. Depmeier, Micropor. Mesopor. Mater. 78 (2005) 217.
[4] E.V. Nazarchuk, S.V. Krivovichev, S.K. Filatov, Radiochemistry 46 (2004) 438.
[5] V.V. Tabachenko, L.M. Kovba, V.N. Serezhkin, Koord. Khim. 10 (1984) 558.
[6] H.T. Stoks, D.M. Hatch, Isotrophy Subgroups of 230 Crystallographic Space Groups, World Scientific, Singapore, 1988.
[7] E.K.H. Salje, Phase Transitions in Ferroelasic and Co-elastic Crystals, Cambridge University Press, 1990.